LAWRENCE
LIVERMORE
NATIONAL
LABORATORY

LLNL-JRNL-855098

Templates of Expected Measurement Uncertainties for (n, xn) Cross Sections

J. R. Vanhoy, R. C. Haight, S. F. Hicks, M. Devlin, D. Neudecker, M. Herman, A. Koning, K. J. Kelley, I. Thompson

September 28, 2023

European Journal of Physcs Nuclear Science and Technologies

Disclaimer

Templates of Expected Measurement Uncertainties for (n, xn) Cross Sections

J.R. Vanhoy[a]*, R.C. Haight[b], S.F. Hicks[c,d], M. Devlin[b], D. Neudecker[b], M. Herman[b], A. Koning[e], K.J. Kelly[b], I. Thompson[f]
[a]U.S. Naval Academy, Annapolis, MD 21402, USA,
[b]Los Alamos National Laboratory, Los Alamos, NM 87545, USA,
[c]University of Kentucky, Lexington, KY 40506, USA,
[d]University of Dallas, Irving, TX 75062, USA,
[e]International Atomic Energy Agency, A-1400 Vienna, Austria,
[f]Lawrence Livermore National Laboratory, Livermore, CA 94551-0808, USA

September 20, 2023

Abstract

A template is provided for evaluating experimental uncertainties for neutron elastic and inelastic scattering cross sections and γ-ray production cross sections from (n, xn) measurements at laboratories with monoenergetic or white neutron sources. A typical range of uncertainties is presented for experiments detecting the scattered neutrons or the resulting de-excitation γ rays based on a survey of available data and input from many experimentalists and theorists with extensive knowledge in the field. Models commonly used to evaluate the resulting cross sections are also discussed. Suggestions are made regarding what experimental and uncertainty information is needed for data evaluations and should be included when reporting experimental (n, xn) cross sections. Uncertainty values and correlations are recommended if these values cannot be estimated for past data from the literature.

1 Introduction

Templates are designed to help experimentalists provide the information necessary for nuclear data evaluations, reviewers in critiquing manuscript submissions, and evaluators in estimating detailed covariances of measured cross sections systematically and efficiently. This template follows from the lead-off paper of Neudecker [1] and discusses neutron-induced reactions where one or more neutrons appear in the exit channel and either neutrons or the associated γ rays are detected. Prompt fission neutron spectra (PFNS), thermal neutron scattering, and neutron capture (n, γ) measurements are explicitly excluded from this discussion and covered in Refs. [2,3].

If only one neutron is emitted, the residual nucleus has the same identity as the target nucleus. If the incoming neutron leaves the target nucleus in its ground state, the process is called elastic scattering. Neutron elastic scattering is often denoted (n, el) or as (n, n_0), and the cross section as σ(n, el). Elastic scattering includes two reaction mechanisms: 1) the incident neutron deflects off the nuclear potential field (direct or shape elastic), or 2) the incident neutron is absorbed by the nucleus and an outgoing neutron emerges with the same kinetic energy as the incident neutron (compound-nucleus elastic).

*E-mail of corresponding author: vanhoy@usna.edu,

The incident neutron may deposit a portion of its energy in the target nucleus. Inelastic neutron scattering that leaves the target nucleus excited is denoted generically as (n, n′), or more specifically as (n, n_k) for its k^{th} excited level.

At sufficiently high incident neutron energies, exit channels such as (n, 2n), (n, 3n), (n, np), ..., as well as continuum neutron emission occur. Description of the reaction mechanism becomes complicated. Direct and compound-nuclear type processes occur, but also pre-equilibrium processes where the system breaks up before statistical equilibrium occurs. During pre-equilibrium, the projectile transfers energy to a small number of nucleons, which in turn can transfer energy to a few other nucleons.

Levels of the residual nuclei usually de-excite through γ-ray emission although there are a few cases where particles are emitted. It is often easiest to detect these γ rays to determine angle-integrated cross sections for neutron scattering to discrete final levels because of the excellent energy resolution of high purity germanium (HPGe) detectors and the ability to know the specific nuclear origin of these γ rays.

A schematic example of the measurement technique discussed in the paper is shown in Fig. 1.

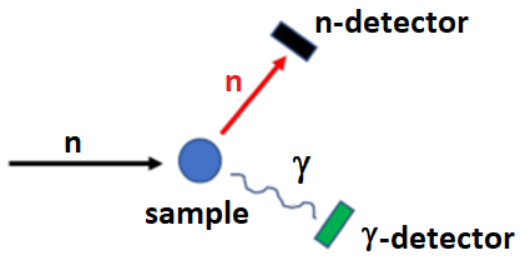

Figure 1: A basic configuration of measurements related to (n, xn) cross sections. Neutrons from the production target are shown entering from the left. Neutrons and γ rays generated by reactions with the sample are recorded by appropriate detectors. The angular dependence of the scattering is recorded by rotating the detectors about the center of the sample in the scattering plane or by using a multiple-detector array.

It is especially difficult to extract elastic scattering differential cross sections at minima in the angular distributions, inelastic scattering where residual levels are not cleanly resolved, neutron emission at low outgoing neutron energies, or measurements with gaseous target samples or data for rare isotopes. A complementary discussion can be found in Ref. [4]. Further information for this template is taken from various sources, namely, Refs. [5–75].

An overview of experimental measurement techniques is presented in Section 2. For convenience in discussing the diverse configurations, equipment, and analysis techniques at many laboratories, we classify them according to the type of neutron production source, either monoenergetic source or broad-band white source. Section 3 discusses the information needed for evaluations with a short explanation of how experimental information impacts theoretical reaction models. Section 4 presents the actual template and provides guidance about why each item is required. The template serves as a checklist and gives reasonable, conservative estimates of uncertainties in cases where specific values are not provided.

2 Measurement Techniques

Many parameters are required to describe and specify the techniques of (n, xn) measurements and the correlations of parameters and results.

In this section, measurement techniques are distinguished according to the neutron source (*i.e.*, "white" versus "monoenergetic") and what particle is measured (*i.e.*, neutrons or the associated γ rays or both in coincidence). The reason for separating techniques according to the neutron source is that there are different geometries at "white" neutron source laboratories and "monoenergetic" neutron source laboratories. These geometries are described in more detail below. Another distinction between the shape of neutron fluences illuminating the scattering sample is to classify them as "divergent" (usually at monoenergetic laboratories) or "planar" (usually at white source laboratories). Although, it should be mentioned that divergent white neutron sources exist, as, *e.g.*, described in Ref. [76].

2.1 Monoenergetic neutron sources

"Monoenergetic" sources produce neutrons using two-body reactions such as ^{3}H(p, n)^{3}He, ^{2}H(d, n)^{3}He, ^{2}H(t, n)^{4}He, ^{3}H(d, n)^{4}He, ^{7}Li(p, n)^{7}Be, ^{1}H(^{7}Li, n)^{7}Be, ^{1}H(^{11}B, n)^{11}C, ^{1}H(^{15}N, n)^{15}O, or ^{1}H(t, n)^{3}He [26,77–81] typically at university Van de Graaff-type accelerator laboratories (TUNL [30–32,43], OU [33,34], UMass Lowell [35], UKY [36–38], LBNL [82], the now-defunct Dynamitron at ANL [83], the LICORNE [84,85], the now defunct Ion Source Facility of LANL [86–88] and JAERI neutron source [89]). These facilities have moderate precision on both the incident- and outgoing-neutron energies. The neutrons emerge at all angles but preferentially in the forward direction due to the center-of-mass motion and any direct component of the reaction mechanism. The samples are placed in this divergent fluence several centimeters from the production target, and the portion of incident neutrons intercepted is determined by the angular size of the sample as viewed from the production target.

2.1.1 Cross section determination

Ratio techniques are used to produce cross sections because they partially compensate for the geometrical effects and do not require the absolute detector efficiency. Recent illustrations of the techniques appear in Refs. [27,37,38,90]. Preliminary differential cross section estimates for emitted neutrons for sample/state X are usually produced by a sequence similar to:

$$\frac{\mathrm{d}\sigma}{\mathrm{d}\Omega}_{X}(\theta) = fW_X(\theta), \tag{1}$$

where $W_X(\theta)$ is the angular variation for scattering, calculated as

$$W_X(\theta) = \frac{Y_X(\theta)}{Y_{FM}\varepsilon(E_{n'})N_X}, \tag{2}$$

and f is the absolute normalization factor determined from the reference reaction. This is often ^{1}H(n, n)^{1}H elastic scattering from a polyethylene sample, with the following form:

$$f = \left\langle \frac{\frac{\mathrm{d}\sigma}{\mathrm{d}\Omega}_{H}(\theta)}{W_H(\theta)} \right\rangle_{\theta}. \tag{3}$$

In these equations, $Y_X(\theta)$ is the yield of emitted neutrons for sample/state X in the main detector, Y_{FM} is the yield of the source neutrons for relative normalization purposes from, e.g., a forward monitor detector, $\varepsilon(E_{n'})$ is the relative detection efficiency for scattered neutrons of energy $E_{n'}$ entering the detector, and N_X is the number of atoms of species X in the sample. The absolute normalization factor f is determined by averaging the given ratio over a set of angles θ. The $\mathrm{d}\sigma/\mathrm{d}\Omega_X(\theta)$ and f values must be corrected for finite sample effects (attenuation, multiple scattering) and all geometrical effects to obtain absolute final cross sections.

2.1.2 Experimental measurements

Figure 2 provides a schematic representation of neutron scattering experiments with monoenergetic neutron sources. Elastic and inelastic scattering and γ-ray emission are studied with this type of setup.

Typically, a pulsed charged-particle beam impinges on a gaseous or solid material where the neutron source reaction occurs. Neutrons emerging from the source scatter off a sample that is hung $\approx$ 3–10 cm from the end of the gas cell. The sample is often a solid or hollow cylinder for symmetry in the scattering plane for the exiting particles and for ease in handling the geometry when making finite sample corrections. A shadow bar prevents source neutrons from going directly to the neutron detector. Because of the divergent character of the source neutrons, it is important to correct for geometrical effects. Contributions to uncertainties from this source-sample configuration with a gas target include: straggling of the incident charged particle in the entrance foil (often Mo or Ta) that separates the main beamline and gas target; the energy spread caused by the source reaction taking place at different locations in the gas cell; and the energy spread caused by the divergent source neutrons interacting at different sample locations. Each of these uncertainties in energy contribute to time spread in the time-of-flight (TOF) peaks; improving the time spread, however, often results in a decrease in count rate, so experimental conditions are optimized for each run. For solid target sources, the thickness of the target contributes to the uncertainty.

The outgoing neutron energy is determined by the TOF of neutrons from the sample to the neutron detector; this TOF is determined by a beam-timing pickoff usually located immediately upstream of the neutron source and the detection of the neutron in the main detector. The TOF is corrected for the time for the beam to hit the gas target and for the short time of each neutron's flight to the sample. The zero time is well determined from the prompt γ-ray peak corrected for the flight time of the γ rays to the detector.

The neutron detector, often a scintillator with excellent timing and pulse shape discrimination (PSD) capabilities, is located $\approx$ 2–10 m from the sample to provide adequate resolution to separate elastic and inelastically scattering groups in the TOF spectra. Unwanted γ-ray events are rejected in these spectra using PSD. The relative efficiency of the detector can be determined experimentally by measuring the angular distribution of the source reaction or it can be calculated. If γ-ray detection is desired, then a γ-ray detector, often a HPGe detector, is placed 1–2 meters from the scattering sample. For γ-ray detection, unwanted neutron events are rejected using TOF techniques, and the efficiency of the detector is determined using γ-ray source standards.

Two examples of background-subtracted TOF spectra obtained with monoenergetic neutron beams are shown in Fig. 3. Differential cross sections are generated by measuring spectra at many angles and using Eqs. [1–3] to deduce the angular dependence of the scattering or reaction.

γ-ray production cross sections can provide information on the non-elastic neutron channels, as well. Here, γ-ray spectra must be measured at many angles and the resulting angular distributions fitted with a Legendre polynomial expansion to obtain the angle-integrated relative production cross section once corrected for detector efficiency and feeding from higher-lying levels. Sometimes the measurements are made at a single angle, 55° or 125° degrees, where the Legendre coefficient P_2 is identically zero, and one can easily deduce the angle-integrated cross sections, if one assumes the a_4 and all higher coefficients are zero. Making this assumption could lead to 5-15% errors near the γ-ray threshold for E2 transitions [39]. (Typically less further above threshold.) This latter technique allows one to consider γ-ray production cross sections for a range of incident neutron energies and to study the excitation function of the γ rays, which is important for developing the level scheme of a nucleus.

If the residual nucleus' level scheme and branching ratios are well known, these γ-ray cross sections can be converted into (n, n_k), (n, 2n), (n, 3n)$\cdots$ cross sections, although this is a subtractive process and uncertainties accumulate quickly. For dense level schemes, nuclear-structure-model calculations are sometimes performed to estimate the γ-ray feeding sequences and direct ground-state γ-ray transitions [7, 8]. Those types of calculations are very dependent on having the level scheme information

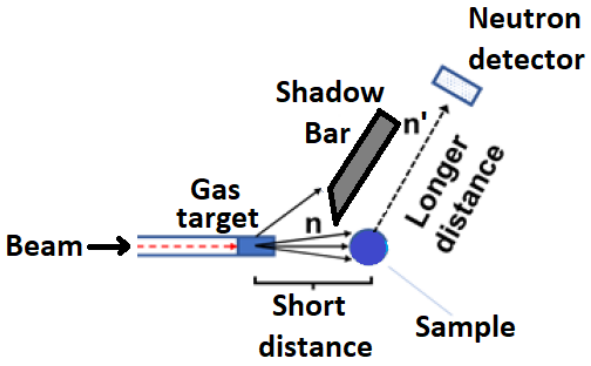

Figure 2: Schematic representation of neutron scattering experiments with monoenergetic neutron sources where only the scattered neutrons are detected. The shadow bar blocks the detector from seeing source neutrons directly. An advanced shadow bar construction is described in Ref. [34]. Measurements are made with sample-in and sample-out.

correct [9].

Gamma-ray production cross sections from (n, xnγ) reactions are an important indicator for the validity of the spin distribution of level density models. As the γ rays cascade down from the continuum to the discrete states, the feeding from the continuum which is driven by spin-dependent level densities determines the low-energy discrete level gamma transitions. Ref. [40] provides a discussion of this effect for ^{238}U(n, n$'\gamma$) reactions. This is important for nuclear data evaluation since the model codes containing these level density models are used to produce complete nuclear data libraries, and also for reactions and nuclides for which no measurements exist.

An additional problem with using γ-ray production cross sections to deduce neutron cross sections is that there are few cross section standards. These measurements are most easily performed relative to the cross sections deduced from the detection of a single γ ray; ^{10}B(n, $\alpha_1\gamma$) (E$_\gamma$ = 0.478 MeV), ^{7}Li(n, n$'\gamma$) (E$_\gamma$ = 0.478 MeV) and ^{48}Ti(n, n$'\gamma$) (E$_\gamma$ = 0.984 MeV) are listed as potential reference cross sections in Ref. [5].

2.2 White neutron sources

"White source" laboratories produce neutrons by spallation (*e.g.* LANSCE [6–12, 42]) or photoproduction (RPI [20, 91–93], GELINA [15–19], nELBE [21–25], ORELA [13, 14], Helios [94, 95]). The neutron fluence is well collimated and very nearly planar at the sample which is illuminated rather uniformly. These are called "white" neutron sources as they produce neutrons with a wide range of energies at the same instant in time; thus, a continuum of neutron energies is incident on the sample. The energy of a particular (incident) event is determined by the TOF from the source to the sample. The scattering sample under study is placed many meters from the neutron source and the fluence has a very small emittance; hence, no shadow bars are necessary in these type of measurements. Direct, absolute cross section measurements can be performed by monitoring the fluence with fission chambers. These facilities generally know the incident neutron energy very precisely, but do not typically measure the energy of the outgoing neutrons. Counterexamples exist and the double time-of-flight method described in Ref. [10] and [96] is implemented in Refs. [23, 97, 98].

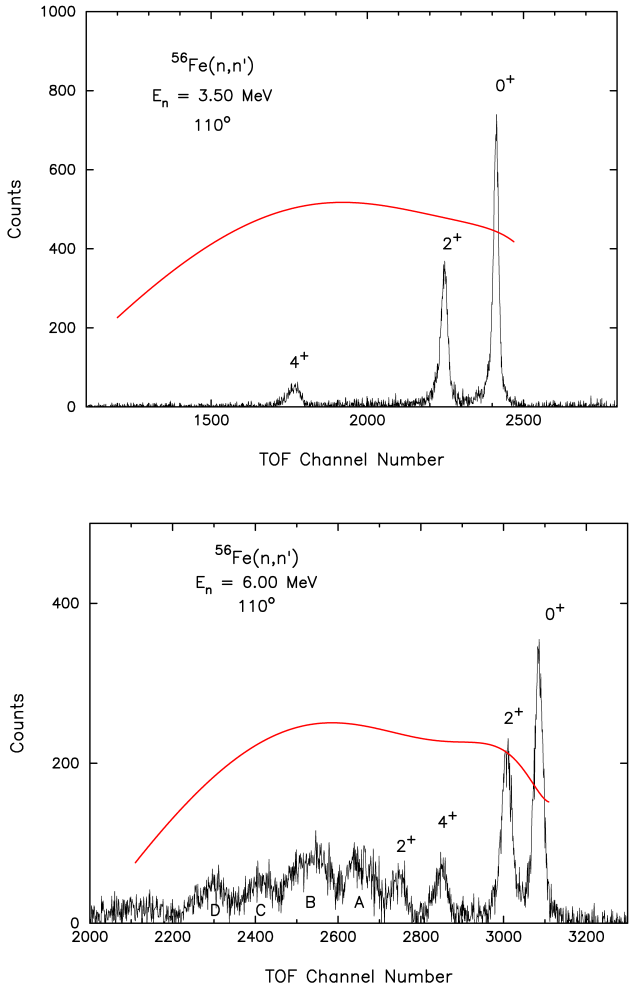

Figure 3: Representative background-subtracted neutron TOF spectra of ^{56}Fe(n, n$_k$) typical of Van de Graaff laboratories; these data are published in Ref. [37]. Peaks are labeled with the residual nucleus spin. The red line is an example of the energy dependent neutron detector efficiency, here displayed as a function of channel number. These spectra illustrate the difficulties encountered in TOF measurements, where typically only scattering from a few low-lying states can be resolved. Clumps of levels (A-D) develop at higher energies and although one knows the levels in each clump from nuclear structure investigations, it is generally not possible to extract the individual contributions. For low mass targets, say A < 40, multiple scattering in the sample creates left-side, lower energy tails and features which make it difficult to extract the yields of neighboring peaks.

2.2.1 Cross section determination

Preliminary γ-ray or neutron differential cross section estimates for detector j at an angle θ_i and incident neutron energy E_k are produced with a formula similar to:

$$\frac{\mathrm{d}\sigma_j}{\mathrm{d}\Omega}(\theta_i, E_k) = \frac{1}{4\pi}\frac{Y_j(E_k)}{Y_{\mathrm{FC}}(E_k)}\frac{\varepsilon_{\mathrm{FC}}\sigma_U(E_k)}{\varepsilon_j}\frac{t_U}{t_s}\frac{A_s}{A_U}\frac{1}{m(E_k)}, \tag{4}$$

where the notation j refers to the γ-ray/neutron detector, FC to the fission chamber, U to the ^{235}U contained in the fission chamber and s to the sample. Y_j is the net peak yield of the examined γ rays/neutrons, Y_{FC} is the fission-chamber yield, ε_j is the absolute detection efficiency for the exit particle at its energy, $\varepsilon_{\mathrm{FC}}$ is the absolute detection efficiency of the fission chamber, t is the thickness

in μg/cm^2 and A is the atomic mass number. The quantity $\sigma_U(E_k)$ is the standard neutron-induced fission cross section of ^{235}U and $m(E_k)$ is the correction factor for multiple scattering. The $\varepsilon_{\rm FC}$ itself can be quite challenging (See *e.g.* Ref. [99]). A detailed discussion of uncertainties and correlations at the laboratory GELINA is available in Ref. [19].

2.2.2 Experimental measurements

White source neutron measurements are further distinguished by what outgoing particle is detected, namely:

- Outgoing neutrons are detected: Figure 4 provides a schematic representation of neutron scattering experiments with a white neutron source. Differential (elastic and discrete inelastic) and double differential cross sections (continuum) can be measured with this technique. The samples are generally cylindrical, although other shapes are occasionally encountered. The neutron detector needs to be fairly close ($\sim$ 1 meter) to the sample for an acceptable counting rate. Some energy discrimination is necessary for the neutron detector, but few neutron detectors have that capability and so often only the highest pulse heights characteristic of neutron elastic scattering are used.

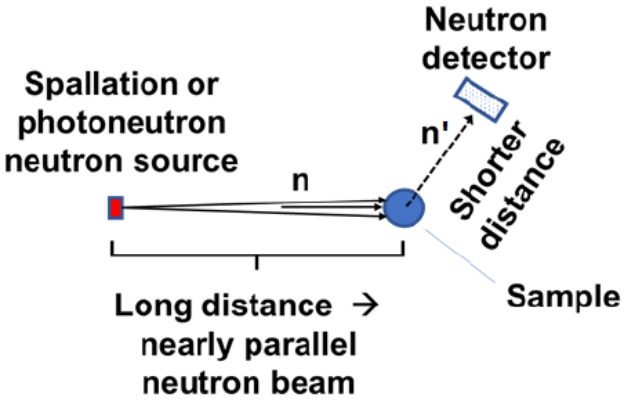

Figure 4: Schematic representation of neutron scattering experiments at a white neutron source facilities where only the scattered neutrons are detected.

  An example of a raw spectrum obtained by a white neutron source measurement at RPI, along with MCNP simulations of the experimental geometry, is shown in Fig. 5.

- Outgoing (discrete) γ rays are detected: Figure 6 provides a schematic representation of neutron inelastic scattering experiments with a white neutron source where the γ ray from the decay of the excited nucleus is detected. In some historical experiments, the γ ray was observed only at 125°, where $P_2 = 0$ in the Legendre polynomial expansion. Assuming that the P_4 Legendre coefficient is zero, measurements at the single 125° detector angle can produce an estimate for the angle-integrated γ-ray production cross section. This assumption is not valid near the level's threshold, and several additional angles are now generally measured to produce a reliable result [15,16,39].

  Partial information on other reactions such as (n, 2n), (n, 3n), (n, p), *etc.*, can be obtained with similar high resolution γ-ray measurements.

  Examples of γ-ray production measurements that yield the (n, n$_k$) cross sections as a function of incident neutron energy are given in Fig. 7 and Fig. 8. Because the same γ ray is detected for every incident neutron energy in this range, uncertainties in the cross sections are highly correlated, and the questions of absorption of γ rays in the sample and of detector efficiency drop

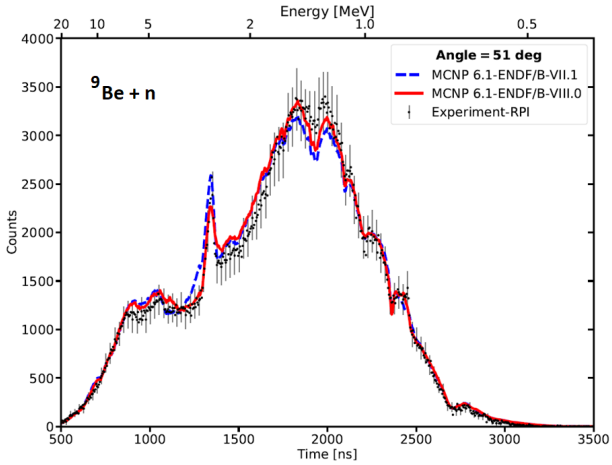

Figure 5: Representative spectrum from neutron scattering measurements on beryllium at RPI that is typical of white neutron source laboratories. The raw measurements are overlaid with MCNP simulations of the experiment geometry [41]. The experimental setup and additional details of neutron scattering measurements at RPI can be found in Ref. [101].

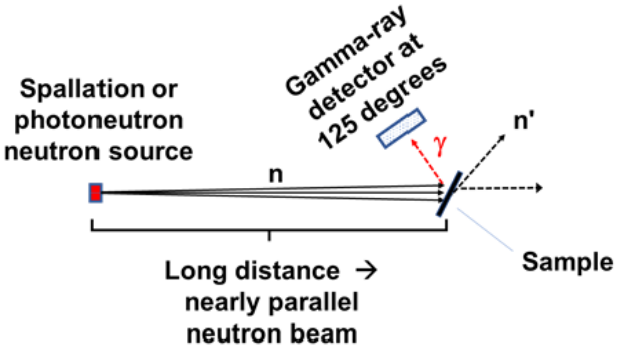

Figure 6: Schematic representation of neutron scattering experiments at a white neutron source where only the γ rays are detected.

out in a relative measurement. This type of measurement is more limited with monoenergetic sources, as the energy resolution of the incident neutrons is typically insufficient to resolve the complex resonance structure of the excitation functions, and the monoenergetic laboratories are unable to cover the wide range of incident neutron energies in a timely fashion.

- A coincidence between neutrons and γ rays is measured: Figure 9 provides a schematic representation of neutron emission, (n, xn), experiments with a white neutron source where both the neutron and an associated γ ray are detected in coincidence [10, 20, 21, 82, 102, 103]. Elastic scattering is not studied with this setup. (Although the neutron-anticoincident neutron data may provide some information on elastic scattering yields.) The incident energy of a particular interaction is determined by the TOF from the source to the sample, which is calculated from the time from the source to the γ-ray detector. The sample can be cylindrical or of some other shape chosen to minimize multiple scattering. The γ-ray detector needs to be fairly close (< 1 meter) from the sample for an acceptable counting rate. The γ-ray detector also needs to have sufficient resolution to resolve the γ-ray transition of interest. The outgoing neutron energy is determined from the TOF from the sample to the neutron detector, with the start signal produced by the γ-ray detector. The neutron detector needs to be relatively close to the sample for an acceptable

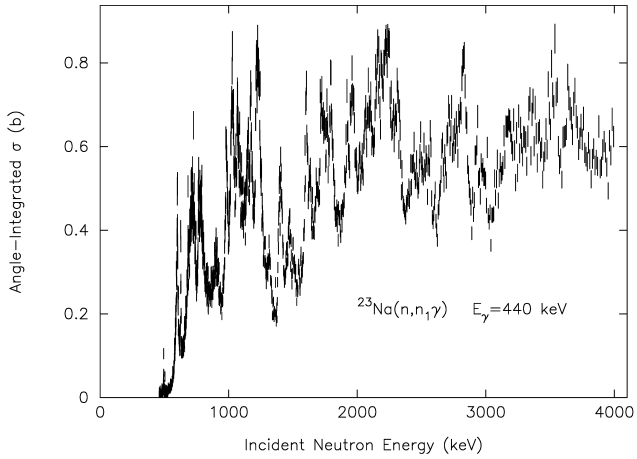

Figure 7: Representative cross sections employing γ-ray detection following the ^{23}Na(n, n$'\gamma$) reaction at the white-source laboratory GELINA to extract level cross sections with fine energy resolution in the resonance region [16].

counting rate. Triple-differential data result from this setup, *i.e.*, differential in incident neutron energy, and energy and angle of the outgoing neutron.

It is conceivable to measure the outgoing neutrons and γ rays in time-coincidence, although in practice the detector solid angles and detector efficiencies lead to extremely small event rates. Historically, n-γ coincidence measurements were performed to provide refined nuclear-structure information. In the modern world, measurements of γ rays can be used to tag the neutrons emitted from specific nuclei for cases of multiple neutron emission. We are only aware of one published n-γ coincidence measurement which directly measured cross sections [104], although preliminary results for ^{27}Al and ^{56}Fe from similar methods were presented at ND2022 [98].

Measurements where neutrons are detected are usually limited to TOF and need a trigger for the outgoing neutron. One major challenge is that the efficiency of the neutron detector needs to be known to obtain the desired observable; it is either calculated or measured with respect to standard cross sections [5] (^{1}H or natural carbon elastic scattering), standard sources (*e.g.*, ^{252}Cf(sf)), or well-studied accelerator-based sources such as ^{2}H(d, n)^{3}He [26]. Multiple scattering and attenuation effects applying to both incident and outgoing neutrons need to be corrected carefully for measurements where neutron detectors are used.

Corrections for multiple scattering of neutrons in the sample (*i.e.*, before a γ ray is emitted) need to be completed in measurements where γ rays are detected. Additionally, γ-ray scattering and absorption, as well as internal conversion, corrections need to be completed for tabulated data, but these corrections should be straight forward [105]. While there are no detector-efficiency standard cross sections for these kinds of γ-ray measurements, several reference cross sections are available, as are calibration sources [5, 106].

3 Information Needed for Evaluations

Experimental data are complied by the 14 teams of the International Network of Nuclear Reaction Data Centers (NRDC) [107]. Data centers compile and sort data using the EXFOR exchange format into reaction types (MT) and type of information (MF) [107, 108].

Reactions of (n, xn) include elastic and inelastic scattering; specific reactions where x = 1, 2, 3...; total neutron emission spectra where there could be several residual nuclei; neutron-gamma-ray correlations in (n, xn-γ) reactions; and neutron-neutron correlations for x > 2. Each of these has

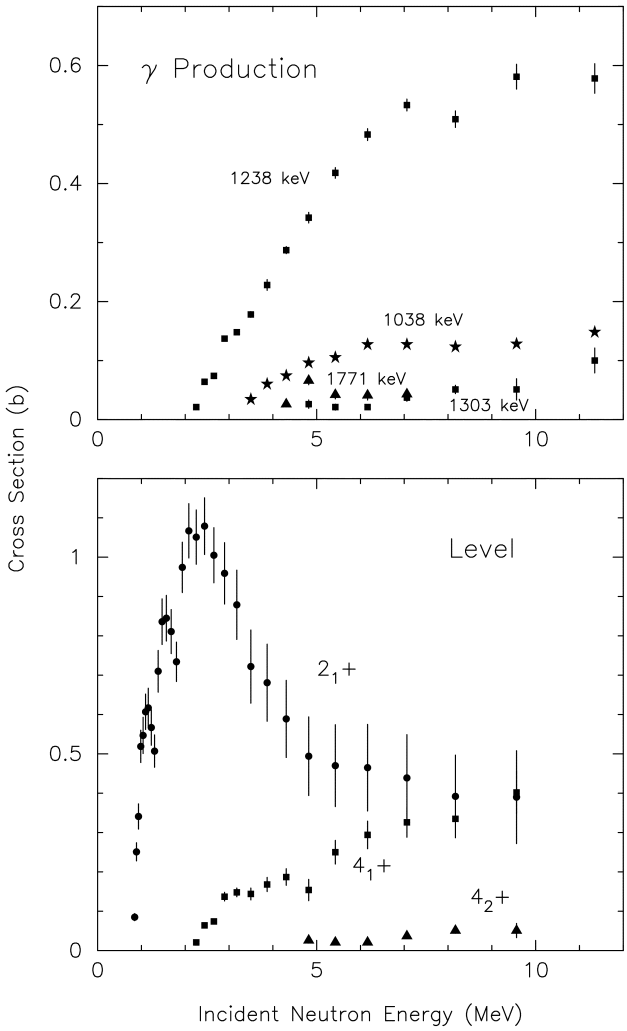

Figure 8: Representative ^{56}Fe results employing γ-ray detection following inelastic neutron scattering from the (n, n$'\gamma$) reaction at the white-source laboratory nELBE to extract level cross sections over a wide range of energies. γ-ray production cross sections are measured (top) and feeding is subtracted to extract level cross sections (bottom) [21]. Other good examples are the ^{56}Fe(n, n$'\gamma$) data of Negret [15] and the ^{23}Na(n, n$'\gamma$) data of Rouki [16] taken at GELINA.

its own existing experimental data base, some extensive, some nearly empty. Here we divide the types of measurements into those that detect elastic and discrete inelastic scattering, those that detect continuum neutron spectra, and those that measure the final states of the residual nuclei.

A complete list of data types can be found in Ref. [108] or online at Ref. [109].

3.1 Elastic and discrete inelastic scattering

At energies below excitation of the first excited state in the target nucleus, (n, xn) comprises only elastic scattering. Elastic cross sections in the low-energy resolved resonance region (RRR) and in the unresolved resonance region (URR) at energies just beyond the RRR are evaluated similarly to the (n, tot) and (n, γ) cross sections in the same energy ranges. A description of this evaluation procedure can be found in Refs. [3] and [110] .

Elastic and discrete inelastic scattering of fast neutrons has been studied mainly with mono-energetic neutron sources. The energy range goes well into the tens of MeV. Analysis of the elastic

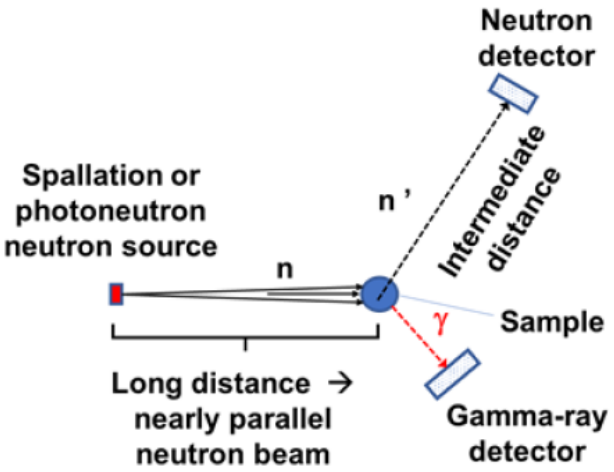

Figure 9: Schematic representation of neutron scattering experiments at a white neutron source lab where the scattered neutrons and γ rays are both detected.

data usually is done through the optical model where the parameters of the model are often assumed to be slowly varying in regions of similar isotopes. Two very popular, readily available codes are TALYS [111] and EMPIRE [112]. More detailed analyses can be carried out if there are data on the analyzing power of the scattering with polarized neutrons [113]. A well-known optical model for near-spherical nuclides is KD03 (Koning-Delaroche) [114], while a powerful optical model for the deformed actinides is DCCOM (Dispersive Coupled-Channel Optical Model) [115]. The resulting optical model parameters have further application in calculations of cross sections of reactions that take place through compound-nuclear processes. The data base for neutron elastic scattering is moderately large at low MeV energies.

Inelastic scattering takes place for incident neutron energies greater than the excitation energy of the first excited state of the target nucleus. As with elastic scattering, TOF techniques are used, and again, good experimental resolution is required. As the nuclear level spacing decreases with increasing excitation energy, the demands for good experimental energy resolution are increased for inelastic scattering to these higher-lying states. The (n, n$'\gamma$) and (n, 2nγ) reaction studies are very important for the theoretical development of spin distributions and level densities. Direct reactions are important in many of these excitations and are often analyzed through Distorted-Wave Born Approximation (DWBA) or Coupled-Channels codes. For certain target nuclei compound-nuclear evaporation must also be considered.

One area where the data are missing or incomplete is in situations where the elastic scattering is not cleanly resolved from inelastic scattering to low-lying states. One example receiving much experimental attention is ^{238}U(n, n) where inelastic scattering to the difficult-to-resolve low-lying excited levels has a large impact upon the power localization in reactor cores [116, 117]. Other examples important for dosimetry applications are scattering to low-lying isomers, such as ^{93}Nb(n, n$'$)^{93m}Nb [118, 119].

An indirect approach to determine inelastic scattering is to measure the gamma rays from the decay of the state in question and then to subtract other processes, namely decay of higher-lying states that populate this state. An example is shown in Fig. 8 for excitation of the first excited state in ^{56}Fe, which can be excited directly by (n, n$'$) excitation as well as by excitation of higher-lying states that gamma-decay to this state. Subtracting the feeding from the higher states from the total production of this state gives the discrete excitation of this state. Of course, this approach does not give the angular distribution of the direct (n, n$'$) scattering, but it does give the cross section for direct excitation.

3.2 Continuum neutron emission

At higher energies where several channels are open for neutron emission, one may refer to "(n, xn)" data where (n, xn) = (n, el) + (n, n′) + (n, 2n) + (n, 3n) + (n, np) + (n, 2np) + (n, nα) + ..., each of which contributes to the total neutron emission. The data base here is spotty, with more measurements at 14 MeV than at other energies. The focus on this energy of incident neutrons is due to the availability of intense 14-MeV neutron sources based on the reaction D+T → n (14 MeV) + α and the application of the same reaction for fusion energy. Again, TOF techniques give data on the spectra of (n, xn) neutron emission as well as the angular distributions of the emitted neutrons. Ring geometry [120] can be used to enhance the counting rate if the material under study is not too expensive, which means that isotopically-enriched samples are often not used. For actinides, where fission is possible, the (n, xn) measurements include prompt fission neutron emission as well as emission from (n, n′), (n, 2n), (n, 3n),... processes. Measurements of double-differential (with respect to outgoing energy and angle) cross section measurements for neutron emission are very rare. Only five entries have even been inserted into the EXFOR DDX category in the past five years [121–125].

The analysis of (n, xn) data is often done with statistical model codes that assume compound-nuclear emission of neutrons. A component of pre-equilibrium neutron emission [127] is also usually required, particularly at higher energies above 10 MeV, to account for the harder emission spectra, and for the angular distributions that are enhanced for neutrons emitted at forward angles.

3.3 Constraints on (n, xn) Reactions

Other types of measurements constrain our knowledge of (n, xn) reactions. Often activation techniques to identify the identify the specific residual nuclei of (n, 2n), (n, 3n) ... reactions. This is not a simple measurements because, for example, the reaction cross sections for ^{93}Nb(n, 2n)^{92}Nb and ^{93}Nb(n, 3n)^{91}Nb must be fit along with the neutron emission spectra to give a database useful for a wide range of applications. Nowadays, activation experiments can be based not only on radiochemical analyses but also on mass spectrometry [3].

Measurement of the prompt gamma rays can give information on the cross section for specific reactions. An example is the ^{239}Pu(n, 2n)^{238}Pu reaction where detection of gamma rays emitted by the excited residual ^{238}Pu nucleus along with theoretical calculations were used to obtain cross sections for this reaction [7].

3.4 Neutron-Gamma and Neutron-Neutron Coincidence

Experiments where prompt gamma rays are detected in coincidence with neutrons reveal the population of particular excited levels as well as to higher states that decay through the particular excited state. More detailed experiments where the scattered neutron is detected in coincidence with a de-excitation gamma ray have a limited presence in EXFOR because of their difficulty. New experiments are in progress to address this lack of coincidence data using the Correlated Gamma-Neutron Array for sCattering (CoGNAC) array at Los Alamos National Laboratory [103].

Most of the exit neutrons in these reactions come from compound nucleus emission, and their energy and almost isotropic angular distributions are well predicted by Hauser-Feshbach models. The first emitted neutron, however, if from pre-equilibrium mechanisms, is more forward peaked and higher in energy than for the later neutrons, so it would be very useful for evaluators if these correlated processes could be experimentally measured.

There are few neutron-neutron coincidence measurements. Activation techniques cannot be used when the residual nuclei are stable. A ^{9}Be(n, n-n) experiment is described in Ref. [100] which measured the energy spectrum of each neutron in the neutron pair.

4 Template

It should be apparent that there are many variations of (n, xn) experiments and data generated. Information produced is used for countless purposes in science and engineering. Evaluators are tasked with producing the best quality data libraries possible. As such, the following items should be discussed or considered in a manuscript:

- Accelerator type and time spreads,
- Neutron production technique,
- How the neutron production was monitored,
- The scattering sample,
- Geometric effects,
- Techniques used to address attenuation and multiple scattering,
- Reference cross sections,
- Detector efficiency,
- Methods used to extract yields from spectra.

This information can aid evaluators in understanding possible shortcomings in the data and maybe even correct the data to a very limited extent in distant future ENDF, JEFF, JENDL, *etc.* libraries.

4.1 Uncertainties

For each of these items, typical experimental details along with representative uncertainty values are briefly summarized in Table I, separated out for monoenergetic neutron beam and white neutron source facilities. Some of the items are explicitly treated in uncertainty and covariance analyses, while others influence the quality of the data but are not easily quantified. Concise discussions of the various items follow the table, where uncertainty values are given in the table. These uncertainty values were estimated based on the expertise of experimenters executing such measurements throughout the years, templates of other observables and the literature cited.

Table I: Typical uncertainty sources encountered in (n, xn) measurements at monoenergetic and white neutron source (WNS) facilities are listed with estimates of typical uncertainty ranges. There is great duplication between the last two columns, but we provide then both to serve as a checklist and to simulate thoughtful comparison for evaluators and experimentalists reporting information.

Uncertainty source	Monoenergetic	WNS
Timing-spread concerns		
Accelerator-beam-pulse width	$<$ 1 ns	$<$ 1 ns
Spread induced by neutron-production target	$\sim$ 1 ns	$\sim$ 1 ns
Spread due to sample size	$<<$ 1 ns	$<<$ 1 ns
Spread due to n/γ-transit time through detector	0.3 ns	0.3 ns
Response time of detector and timing electronics	$\sim$ 10–20 ns	$\sim$ 10–20 ns
TOF determination	$<$ 100 ps	$<$ 100 ps
Deadtimes	Varies	Varies
Neutron-production target		
Overall (need full descrip. includ. cooling)	1%	$\sim$ 1%

Neutron-flux monitoring		
Fission chambers: deposit thickn. & uniform.	$\sim$ 1% (see [99])	$\sim$ 1% (see [99])
Fission chambers: σ_U(n, f)	$\sim$ 1% (see [5])	$\sim$ 1% (see [5])
Long counters	1–2%	N/A
Proton-recoil telescopes	1–2% (see [126])	1–2% (see [126])
Liquid scintillators (For mono.)	1%	N/A
Scintillators (*e.g.*, ^{6}Li-glass)	1%	< 1%
Sample		
Isotopic enrichment	< 1%	< 1%
Contaminants / Secondary contents	$\sim$ 1%	$\sim$ 1%
Chemical/Mechanical form and shape	$\sim$ 1%	$\sim$ 1%
Mass	<<1%	<<1%
Material uniformity	$\sim$ 1%	$\sim$ 1%
Dimensional measurements	0.3%	0.3%
Geometric effects		
Source-sample geometry	<3 %	<< 1%
Sample-detector geometry	$\sim$ 2%	$\sim$ 2%
Detector size & positioning	$\sim$ 2%	$\sim$ 2%
Incident-neutron energy spread	^{7}Li(p, n) $\sim$ 1%, ^{3}H(p, n) 2–5%, ^{2}H(d,n) 2–6%	<< 1%
Attenuation & multiple scattering		
Method used to perform corrections	<5%	<5%
nσ (number density $\times$ cross section)	0.3%	0.3%
Monte Carlo unc. (statistics & methods)	$\sim$ 1%	$\sim$ 1%
Atomic-data uncertainties	$\sim$ 1%	$\sim$ 1%
Nuclear-data uncertainties	Varies	Varies
Standard or reference cross sections		
^{1}H(n, n), ^{56}Fe(n, n$'\gamma$) (jitter), ^{48}Ti(n, n$'\gamma$) ^{7}Li(n, n$'\gamma$), ^{12}C(n, n), ^{235}U(n, f), ^{252}Cf (sf)	From nuclear-data libraries	From nuclear-data libraries
Detector efficiency (neutrons)		
Scintillators, via direct-measurement methods	$\sim$ 3%	$\sim$ 3%
Scintillators, via simulations	$\sim$ 3%	$\sim$ 3%
Detector efficiency (γ rays) [3]		
<0.2 MeV	4%	4%
0.2-2.6 MeV	2%	2%
>2.6 MeV	5%	5%
Ability to extract yields from spectra		
n-TOF spectra, elastic peak	<2%	Limited by counting statistics
n-TOF spectra, inelastic peaks	1–10%	
Continuum-neutron-emission spectra	<20%	

For planar neutron fluences: The time structure of the accelerator, production target material and geometry effects, beam tubes and flight paths, and any beam filters utilized should be specified as this determines the incident neutron energy spectrum. The incident neutron energy for an event is determined by TOF and that requires measurement of the flight path length through the beam tubes and the time the neutron takes to traverse that length. Usually the length is deduced from known transmission resonances in materials that can be placed in the beam. The uncertainty in the beam energy thus depends on the uncertainties in the energies of these transmission resonances, which can

be very small. The other contribution to the uncertainty in the incident neutron energy is the timing uncertainty of the detector. To take nominal values, for a 10 m flight path and a timing uncertainty of 1 ns, the uncertainty in the neutron energy for a 10 MeV neutron is 0.088 MeV.

For divergent neutron fluences: The time spread of the incident beam pulses and details of the gas target construction, gas pressures, cooling of the target, and dimensions and position of the sample with respect to the neutron source are required as these items influence overall energy spreads, time spreads, backgrounds, TOF-spectrum quality, and geometrical corrections. The flight path to the detector and detector/shielding geometry should also be reported.

For neutron production with gas cells, the entrance foil, gas, and auxiliary cell materials are important concerns. The entrance foil degrades the accelerator beam energy and can cause errors in reporting the average incident particle energy. The energy dispersion caused by the entrance foil is usually small compared to the effects from the gas. The uniform energy loss along the length of the gas cell is often the major contribution to the neutron production energy spread at low incident neutron energies, where the loss is typically a few percent of the incident beam energy. Neutron energies vary according to the production location in the gas and emission angle at that location. The spread of neutron energies over the scattering sample because of this neutron fluence divergence must also be considered, as it has an increasing contribution to the energy spread as the accelerator beam energy increases. Overall the energy spread due to straggling of the incident charged particle in the entrance foil, neutron production location in the source, and geometry of the source-sample configuration ranges from a few 10s of keV to a few 100s of keV depending on entrance foil thickness and material, gas cell pressure, and source-sample geometry, as well as the incident neutron energy.

Stopper disks and liners may add small tails to peaks in the neutron spectrum due to scattering off these and other auxiliary materials in the immediate vicinity of the gas cell. Gas contamination can also be a problem with deuteron beams, as the (d, n) production can be significant on trace amounts of C, N, and O. Secondary (d, n) neutron groups can be a problem at high incident energies because of deuteron breakup on gas-cell materials or beam-line components.

Fast neutrons are often made with thin lithium compound deposits and the ^{7}Li(p, n)^{7}Be reaction. The energy spread of neutrons is adjusted via the thickness of the compound layer. A worry is heating of the layer and subsequent evaporation, which in turn alters the average beam energy and spread. For proton beam energies above 2.4 MeV, the ^{7}Li(p, n)^{7}Be source reaction has two neutron groups due to the ground state and the low-lying excited state (0.429 MeV) of the residual ^{7}Be nucleus. For some experiments, the two groups can be resolved. For other experiments (such as around 50 MeV), they are treated as one group.

Neutron flux monitoring: Neutron flux monitoring is performed with fission chambers, BF_3 proportional counters, long counters, or forward monitors, while the latter three monitors are often used at facilities using gas or solid targets as sources.

Fission chamber limitations are the uniformity of the ^{235}U or ^{238}U deposit, knowledge of the (n, f) cross sections, counter gas stability, and electrical effects related to the fission chamber construction. Templates of uncertainty values associated with typical absolute (n, f) cross section measurements suffering from similar issues are given in Ref. [99].

Long counters [44] are often used for excitation function measurements where it is not practical to make detailed efficiency calibrations as a function of beam energy and neutron scattering angles. The long counter has a slowly varying energy response with understood deviations [45]. Recent studies relating to long counter performance can be found in Ref. [46]. Long counters are often designed with simulations [47].

Forward monitors are scintillator detectors capable of TOF and PSD discrimination. They are typically used with ratio methods when performing cross section measurements. Fixed location forward

monitors are best used for angular distribution measurements as their efficiency changes with neutron energy. Scintillation detectors are discussed below.

While some references cite detector efficiency uncertainties smaller than 1%, 1–2% is recommended as a reasonable estimate in case these uncertainties were not reported for an experiment in the distant past.

Detector-response function or efficiency: A number of methods are employed to determine detector-response functions or the efficiency [48]. The efficiencies may be relative (arbitrary units) or absolute (normalized to 100%).

γ-ray detector efficiencies are well determined using standard radioactive sources (*e.g.*, ^{22}Na, ^{56}Co, ^{57}Co, ^{137}Cs ^{152}Eu, ^{203}Hg, ^{226}Ra) for photon energies between ∼120 keV and 2.5 MeV. It is difficult to obtain precise efficiencies outside this range as is highlighted in Ref. [3].

For neutron detectors, the technique employed depends on the location of features in the electronic-response curve. For scintillator materials, the type of material and thickness are also important considerations. Just above the low-energy thresholds, efficiencies are sensitive to the electronic settings, electronic noise, pileup, and threshold effects associated with the choice of discriminator modules [49–51]. Some facilities use neutron MCNP [132]/GEANT [52,53,59] simulations including SCINFUL [54] and POLIMI [55–57] or deterministic calculations.

Other facilities determine neutron detector efficiencies using differential cross section standards ^{3}H(p, n)^{3}He, ^{2}H(d, n)^{3}He, and ^{1}H(n, n)^{1}H [5]; known emission spectra, ^{27}Al(d, n)^{28}Si [58], or a radioactive source spectrum shape (*i.e.*, ^{252}Cf PFNS) [60–66]. For fission chamber monitors, information on the chamber construction and geometry and an evaluation of the ^{235}U or ^{238}U deposit thickness and uniformity are desired.

Sources of backgrounds: Background sources and their impact upon detectors and sample illumination are similar to uncertainties encountered in Refs. [3] and [2] and can be adopted from there.

Scattering samples: The mass and chemical and isotopic compositions and the uniformity of scattering samples are generally extremely well known, hence, the low uncertainty values in Table I. However, it is important to include this information in publications and reports.

Geometric effects: Compromises must be made between count rates, timing and energy resolution, shielding, positioning of equipment, *etc.*, and these lead to geometric effects.

At Van de Graaff laboratories, the scattering sample is placed close to the neutron production source. The source size, source-to-sample spacing, and sample size impact the energy spreads, TOF spectra, and multiple-scattering and attenuation corrections, and it is important to provide this information in a manuscript.

Some measurements place the detectors very close to the scattering sample, effectively summing over observation angles. In these situations, details of the detector geometry and position must be given used perform directional-correlation attenuation corrections as outlined in Refs. [129,130] and [131].

Recommended standards and reference cross sections: Detailed disccusions of standards and refererence cross sections used to deduce absolute cross sections are discussed in Refs. [5, 67]. The reactions ^{1}H(n, n), ^{6}Li(n, t), ^{10}B(n, α), ^{10}B(n, $\alpha_1\gamma$), $^{\rm nat}$C(n, n), Au(n, γ), ^{235}U(n, f) and ^{238}U(n, f) are considered high-quality standard cross sections to be used in detector calibration, neutron flux measurement, and cross section normalization. These reactions are established standards only in a limited energy range which may not be sufficient for measurements being performed.

Other cross sections are denoted as reference cross sections. Examples include ^{56}Fe(n, n$'\gamma$), ^{48}Ti(n, n$'\gamma$), ^{7}Li(n, n$'\gamma$), ^{238}U(n, γ), ^{239}Pu(n, f) cross sections. Others include the Maxwellian spectrum

averaged Au(n, γ) cross section at 30 keV and the ^{252}Cf spontaneous fission neutron spectrum. At few MeV energies, reference cross sections may exhibit very narrow resonance fluctuations (jitter) and manuscripts should comment on the averaging technique utilized.

Extracting yields: Figure 3 above illustrates common difficulties in extracting yields from spectra. At Van de Graaff type laboratories (Fig. 3), the incident neutrons are usually considered monoenergetic and the TOF of exit-channel neutrons is measured. The peak shapes are not Gaussian, but include left-side tails, shelves, and other features and small right-side tails. Because of this, yield uncertainties tend to be dominated by the ability to fit the TOF spectrum rather than counting statistics. Short left- and right-side tails may be due to beam pulse tuning or the gas cell issues discussed previously. Examining the "γ flash" generated in the sample will help identify short-tail issues. Stronger left-side features are due to multiple scattering in the sample and imperfect treatment of background processes in the room, collimation and shielding, and the sample.

Notice that peaks from each n_k exit channel (Fig. 3) have slightly different shapes; this distortion is caused because the spectra are recorded as a function of time rather than energy. Another common problem occurs when the first excited state is not well resolved from the elastic scattering peak, as seen with ^{56}Fe in the bottom panel of Fig. 3. The peaks for the n_0 and n_1 channels will overlap and the yield of the n_1 channel will depend on how the left-side features of the n_0 channel are fitted. In cases of significant ambiguity, it is recommended to report cross section estimates for the combined $n_0 + n_1$ exit channels. This problem is even more pronounced when the cross section to the first exited state is small relative to that for elastic scattering, as it is for ^{23}Na [38].

The spectrum for ^{56}Fe (Bottom panel, Fig. 3) also illustrates the situation for additional exit channels. There is a good chance of separating the yields of the 0^+, 2^+ and 4^+ channels with slightly larger uncertainty but the cross sections to the higher levels must be treated collectively.

At white neutron source laboratories [128] (Fig. 4), separation of elastic and inelastic scattering is easy if the incident neutron energy is below the energy of the first excited state of the target nucleus. The separation is also possible at somewhat higher energies. Inelastic neutron scattering can be triggered by γ rays from the excited states. Double TOF experiments are being perfected, examples being Refs. [10, 20, 82].

Attenuation and multiple-scattering corrections: Finite sample corrections, such as self-absorption, attenuation and multiple scattering, are major concerns for neutron data. Scattering sample dimensions tend to be a few centimeters and the mean free path ($1/\mathrm{n}\sigma$) for collisions of few MeV neutrons tends to be comparable or up to ~20 cm. Both incoming- and exit-channel neutrons suffer attenuation in the sample, which reduces the anticipated yield in the detector. Multiple scattering deflects neutrons which would have missed the detector into it and therefore increases the reaction yield. In addition, multiple-scattered neutrons of single spectra are degraded in energy and create the low-side features on TOF peaks discussed previously. If inelastic scattering is involved, multiple-scattered neutrons may have an energy in excess of neutrons scattered once. Depending on the situation, attenuation and multiple scattering could be up to a $\sim$ 20% correction and in data measured many decades ago could have simply been assumed to cancel.

One approach to tackle these finite sample corrections is based upon the foundational references [68–73] or whole-experiment simulations using codes such as MCNP [132] or GEANT [52, 53, 59].

Two notable codes used at the Van de Graaff laboratories are MULCAT [74, 75] and EFFIGY [27–29]. These are guided/forced Monte Carlo implementations using approaches described in the foundational references.

Simulations of experimental conditions tend to be used at spallation and photo-production laboratories [133]; these simulations are also very useful for optimizing and analyzing experiments with monoenergetic neutron sources. Simulations rely on evaluated nuclear data files typically from ENDF/B, JENDL, or JEFF. Versions of these data files are updated periodically and there could be differences

for specific applications. Manuscripts should reference the evaluated nuclear data file version or the detailed information for specific isotopes utilized.

For γ-ray emission measurements used to deduce neutron cross sections, attenuation of γ rays in the sample needs to be taken into account. Many such measurements are based on detection of the same energy γ rays over a range of incident neutron energies. Thus, attenuation of the γ rays and internal conversion must be included when deducing neutron inelastic scattering cross sections from γ-ray production cross sections. Both processes are of greater importance for low-energy γ rays.

4.2 Correlations

The previous section concentrates on myriad numbers of *primary parameters* of an experiment and their uncertainties. The results of an experiment are *derived parameters*, two examples being an energy-dependent cross section for a reaction channel or an emission spectrum. The connection between primary parameters and derived parameters is by no means simple and may not be expressible via mathematical functions. One goal of data evaluators is to understand the quality of results. The uncertainties and correlations of primary parameters are managed by building a covariance matrix. Examples and applications of this technique are described in Refs. [1, 134] and [135].

Table II provides information on estimating correlation values.

Table II: Typical uncertainty sources encountered in (n, xn) measurements are tabulated with special emphasis on shapes of correlations. The notation Exp_i refers to different datasets from the same laboratory.

Unc. source	$\mathrm{Cor}(\mathrm{Exp}_i, \mathrm{Exp}_i)$	$\mathrm{Cor}(\mathrm{Exp}_i, \mathrm{Exp}_j)$ $i \neq j$
Timing-spread	From TOF $\rightarrow E_{\mathrm{out}}$ transformation	$\neq 0$ for same facility/detector
Neutron-production target	Full	$\neq 0$ for same facility
Neutron-flux monitoring	Gaussian	$\neq 0$ for same facility/detector
Sample	Full	$\neq 0$ for similar target/ methods
Geometric effects	Full	$\neq 0$ for same facility
Attenuation & multiple scatt.	Gaussian	Facility/ methods dependent
Standards & references	From libraries	From libraries
Detector efficiency (neutrons)	Gaussian	Depends on efficiency determination
Detector efficiency (γ rays)	Full	Depends on efficiency determination
Extracting yields	Gaussian	$\neq 0$ for same facility/detector

Correlation shapes for uncertainty sources are recommended in the table in case no information can be found in an original journal article to estimate those. The reasoning for assuming these approximate shapes is described at length in Refs. [1], [2], and [3]

An entry 'Full" means that all correlation coefficients are one between all data at different angles or energies. A "Gaussian" correlation shape between matrix entries i and j was defined in Ref. [135] as

$$\mathrm{Cor}_{ij} = \exp\left\{ -\left[\frac{c(x_i - x_j)}{\max(x_i, x_j)} \right]^2 \right\}, \tag{5}$$

where x_i and x_j either correspond to outgoing neutron energies or angles. The value c is a scaling parameter and can be chosen with values between 0 (full correlation) and 1 (stronger correlation between values with x_i and x_j being close together, and weaker if they are far apart).

5 Conclusions

Templates of uncertainties associated with (n, xn) measurements resulting in neutron elastic and inelastic scattering cross sections, neutron inelastic cross sections deduced from γ-ray production cross sections, and (n, 2n), (n, 3n), (n, p)... cross sections were presented in this work. Ranges of uncertainties expected for known experimental sources of errors and estimated correlations were presented separately for measurements conducted at laboratories that use monoenergetic neutron sources and for those that use white neutron sources. The uncertainties are estimated from relevant publications, online data bases such as EXFOR, and from scientists and engineers with broad experience in the field of neutron physics. In addition to the template of uncertainties, a discussion of experimental observables, their uncertainties, and how they can best be included in the publication of experimental data for evaluators to use the results most effectively in the evaluation process.

Conflicts of Interest

The authors declare that they have no competing interests to report.

Funding

Research at the University of Kentucky Accelerator Laboratory is supported by contracts from the Office of Nuclear Physics awards DE-20SSC000056, DE-SC0021243, DE-SC0021175, and DE-SC0021424.

Work at Los Alamos National Laboratory was carried out under the auspices of the NNSA of the U.S. Department of Energy under contract 89233218CNA000001.

This work was performed in part under the auspices of the U.S. Department of Energy by Lawrence Livermore National Laboratory under Contract DE-AC52-07NA27344.

Data availability statement

The data that are associated with this manuscript are all within its main text and tables or referenced appropriately.

Author contribution statement

JRV and RCH complied references and information, produced many versions of the original manuscript, and were the leads throughout the project. SFH joined to assist incorporating material and to make the discussions more coherent and precise. MD provided much development for the white source sections. DN provided the original vision for the Template projects and guidance to the team for this manuscript. MH, AK, KK, and IT contributed discussions specific to their experience. All authors reviewed and proposed edits to the manuscripts. All authors were involved in investigations and data curation associated with the article and discussions on uncertainty quantification for (n, xn) cross section measurements.

References

[1] D. Neudecker, A.M. Lewis, E.F. Matthews *et al.*, "Templates of Expected Measurement Uncertainties,"accepted for publication in Europ. Phys. J. N (8 August 2023).

[2] D. Neudecker, M. Devlin, R.C. Haight *et al.*, "Templates of Expected Measurement Uncertainties for Prompt Fission Neutron Spectra,"submitted to Europ. Phys. J. N (2023).

[3] A.M. Lewis, D. Neudecker, A.D. Carlson *et al.*, "Templates of Expected Measurement Uncertainties for Capture and Charged-Particle Production Cross Section Observables,"submitted to Europ. Phys. J. N (2023).

[4] R.C. Block, Y. Danon, F. Gunsing, *et al.*, *Neutron Cross Section Measurements.* Handbook of Nuclear Engineering, Springer Verlag **1**, pp. 1–81 (2010). https://doi.org/10.1007/978-0-98149-9_1.

[5] A.D. Carlson, V.G. Pronyaev, R. Capote *et al.*, "Evaluation of the Neutron Data Standards," Nucl. Data Sheets **148**, 143–188 (2018). https://doi.org/10.1016/j.nds.2018.02.002.

[6] P.W. Lisowski, C.D. Bowman, G.J. Russell *et al.*, "Los Alamos National Laboratory Spallation Neutron Sources," Nucl. Sci. Eng. **106**, 208–218 (1990). https://doi.org/10.13182/NSE90-A27471.

[7] L.A. Bernstein, J.A. Becker, P.E. Garrett *et al.*, "^{239}Pu(n, 2n)^{238}Pu Cross Section Deduced using a Combination of Experiment and Theory," Phys. Rev. C **65**, 021601(R) (2001). https://doi.org/10.1103/PhysRevC.65.021601.

[8] L.A. Bernstein, D.E. Archer, J.A. Becker *et al.*, "Studying the Role of Nuclear Structure Effects in Neutron-Induced Reactions using GEANIE at LANSCE," Nucl. Phys. A **682**, 404c (2001). http://dx.doi.org/10.1016/S0375-9474(00)00667-9.

[9] G.P.A. Nobre, "Impact of Experimentally Constrained Level Densities on (n, n$'\gamma$)," presentation at WINS2018 Workshop on Inelastic Neutron Scattering, Predeal, Romania, 19–21 Sept 2018.

[10] D. Rochman, R.C. Haight, J.M. O'Donnell *et al.*, "Neutron-induced Reaction Studies at FIGARO using a Spallation Neutron Source," Nucl. Instrum. Meth. Phys. Res. Sec. A **523**, 102–115 (2004). https://doi.org/10.1016/j.nima.2003.12.026.

[11] N. Fotiades, M. Devlin, R.C. Haight *et al.*, "α and 2p2n Emission in Fast Neutron-induced Reactions on ^{60}Ni," Phys. Rev. C **91**, 064614 (2015). http://dx.doi.org/10.1103/PhysRevC.91.064614.

[12] R.O. Nelson, "Cross Section Measurements at LANSCE for Defense, Science and Applications," EPJ Web Conf. **93**, 06002 (2015). http://dx.doi.org/10.1051/epjconf/20159306002 .

[13] K.H. Guber, L.C. Leal, R.O. Sayer *et al.*, "New Neutron Cross-section Measurements at ORELA and their Application in Nuclear Criticality Calculations," Nucl. Instrum. Meth. Phys. Res. Sec. B **241**, 218–222 (2005). http://dx.doi.org/10.1016/j.nimb.2005.07.083.

[14] H. Derrien, J.A. Harvey, K.H. Guber *et al.*, "Average Neutron Total Cross Sections in the Unresolved Energy Range from ORELA High-resolution Transmission Measurements," Oak Ridge National Laboratory Report ORNL/TM-2003/291 (2004).

[15] A. Negret, C. Borcea, Ph. Dessagne *et al.*, "Cross-section Measurements for the ^{56}Fe(n, xnγ) Reactions," Phys. Rev. C **90**, 034603 (2014). https://doi.org/10.1103/PhysRevC.90.034602.

[16] C. Rouki, P. Archier, C. Borcea *et al.*, "High Resolution Measurement of Neutron Inelastic Scattering Cross-sections for ^{23}Na," Nucl. Instrum. Meth. Phys. Res. Sec. A **672**, 82–93 (2012). https://doi.org/10.1016/j.nima.2012.01.004.

[17] D. Ene, C. Borcea, S. Kopecky *et al.*, "Global Characterisation of the GELINA Facility for High-resolution Neutron Time-of-flight Measurements by Monte Carlo Simulations," Nucl. Instrum. Meth. Phys. Res. Sec. A **618**, 54–68 (2010). https://doi.org/10.1016/j.nima.2010.03.005.

[18] W. Mondelaers and P. Schillebeeckx, "GELINA: A Neutron Time-of-flight Facility for High-resolution Neutron Data Measurements," Notiziario Neutroni eLuce di Sincrotrone **11**, 19 (2006). Accessible online at https://issuu.com/nnls/docs/nnls_vol11-n2_06.

[19] A. Plompen and A. Negret, "Uncertainties and Covariances for Inelastic Scattering Data—A Status Report," JRC Scientific and Technical Reports EUR 25208 EN (2011). https://doi.org/10.2787/58803.

[20] A. Daskalakis, E. Blain, G. Leinweber *et al.*, "Assessment of Beryllium and Molybdenum Nuclear Data Files with the RPI Neutron Scattering System in the Energy Region from 0.5 to 20 MeV," EPJ Web of Conf. **146**, 11037 (2017). https://doi.org/10.1051/epjconf/201714611037.

[21] R. Beyer, R. Schwengner, R. Hannaske *et al.*, "Inelastic Scattering of Fast Neutrons from Excited States in ^{56}Fe," Nucl. Phys. A **927**, 41–52 (2014). http://dx.doi.org/10.1016/j.nuclphysa.2014.03.010.

[22] R. Beyer, E. Birgersson, Z. Elekes *et al.*, "Characterization of the Neutron Beam at nELBE" Nucl. Instrum. Meth. Phys. Res. Sec. A **723**, 151–162 (2013). https://doi.org/10.1016/j.nima.2013.05.010.

[23] E. Pirovano, R. Beyer, M. Dietz *et al.*, "Cross Section and Neutron Angular Distribution Measurements of Neutron Scattering on Natural Iron," Phys. Rev. C **99**, 024601 (2019). https://doi.org/10.1103/PhysRevC.99.024601.

[24] A.R. Junghans, R. Beyer, Z. Elekes *et al.*, "Fast-neutron Induced Reactions at the nELBE Time-of-flight Facility," Nucl. Data Sheets **119**, 349–352 (2014). http://dx.doi.org/10.1016/j.nds.2014.08.096.

[25] A.R. Junghans, E. Altstadt, C. Beckert *et al.*, "The nELBE Neutron Time-of-flight Facility," 2008 IEEE Nuclear Science Symposium Conference Record **N42-3**, 2909–2911 (2008).

[26] M. Drosg, "DROSG-2000v12.01: Neutron Source Reactions. Data Files with Three Computer Codes for 60 Accelerator -Based Two-body Neutron Source Reactions," IAEA Report IAEA-NDS-87 Rev. 10 (Feb. 2017), and "https://www-nds.iaea.org/public/libraries/drosg2000/ "(2003).

[27] S.M. El-Kadi, C.E. Nelson, F.O. Purser *et al.*, "Elastic and Inelastic Scattering of Neutrons from ^{54,56}Fe and ^{63,65}Cu. (I). Measurements from 8 to 14 MeV and a Spherical Optical Model Analysis," Nucl. Phys. A **390**, 509–540 (1982). http://dx.doi.org/10.1016/0375-9474(82)90281-0.

[28] H.H. Hogue, P.L. von Behren, D.W. Glasgow *et al.*, "Elastic and Inelastic Scattering of 7- to 14-MeV Neutrons from Lithium-6 and Lithium-7," Nucl. Sci. Eng. **69**, 22–29 (1979). http://dx.doi.org/10.13182/NSE79-A21281

[29] H.H. Hogue, P.L. von Behren, D.H. Epperson *et al.*, "Differential Elastic and Inelastic Scattering of 7- to 15-MeV Neutrons from Beryllium," Nucl. Sci. Eng. **68**, 38–42 (1978). http://dx.doi.org/10.13182/NSE78-A27268

[30] J.P. Delaroche, S.M. El-Kadi, P.P. Guss *et al.*, "Elastic and Inelastic Scattering of Neutrons from ^{54,56}Fe and ^{63,65}Cu. (II). Scattering and Nuclear Structure Effects from Coupled Channels Calculations," Nucl. Phys. A **390**, 541–560 (1982). http://dx.doi.org/10.1016/0375-9474(82)90282-2.

[31] S.G. Glendinning, S. El-Kadi, C.E .Nelson *et al.*, "Elastic and Inelastic Neutron Cross Sections for Boron-10 and Boron-11," Nucl. Sci. Eng. **80**, 256–262 (1982). http://dx.doi.org/10.13182/NSE82-A21429.

[32] S.G. Glendinning, S. El-Kadi, C.E. Nelson *et al.*, "Neutron Elastic Scattering Cross Sections for ^{16}O between 9 and 15 MeV," Nucl. Sci. Eng. **82**, 393–399 (1982). http://dx.doi.org/10.13182/NSE82-A21453.

[33] S. Mellema, R.W. Finlay and F.S. Dietrich, "Neutron Inelastic Scattering from ^{54,56}Fe," Phys. Rev. C **33**, 481 (1986). http://dx.doi.org/10.1103/PhysRevC.33.481.

[34] R.W. Finlay, C.E. Brient, D.E. Carter, A. Marcinkowski, S. Mellema, G. Raners-Pehrson, J. Rapaport *et al.*, "The Ohio University Beam Swinfer Facility," Nucl. Instrum. Meth. Phys. Res. **198**, 197–206 (1982). https://doi.org/10.1016/0167-5087(82)90256-3.

[35] D.R. Donati, S.C. Mathur, E. Sheldon *et al.*, "Cross Sections, Angular Distributions, and Magnetic Substate Populations in the ^{23}Na(n, n$'\gamma$) Reaction," Phys. Rev. C **16**, 939 (1977). http://dx.doi.org/10.1103/PhysRevC.16.939.

[36] J.R. Vanhoy, S.H. Liu, S.F. Hicks *et al.*, "^{54}Fe Neutron Elastic and Inelastic Scattering Differential Cross Sections from 2–6 MeV," Nucl. Phys. A **972**, 107–120 (2018). http://dx.doi.org/10.1016/j.nuclphysa.2018.02.004.

[37] A.P.D. Ramirez, J.R. Vanhoy, S.F. Hicks *et al.*, "Neutron Scattering Cross Section Measurements for ^{56}Fe," Phys. Rev. C **95**, 064605 (2017). http://dx.doi.org/10.1103/PhysRevC.95.064605.

[38] J.R. Vanhoy, S.F. Hicks, A. Chakraborty *et al.*, "Neutron Scattering Differential Cross Sections for ^{23}Na from 1.5 to 4.5 MeV," Nucl. Phys. A **939**, 121–140 (2015). http://dx.doi.org/10.1016/j.nuclphysa.2015.03.006.

[39] J.R. Vanhoy, A.P. Ramirez, D.K. Alcorn-Dominguez, S.F. Hicks, E.E. Peters, M.T. McEllistrem, S.Mukhopadhyay, S.W. Yates *et al.*, "Inspection of ^{56} Fe γ-Ray angular distributions as a function of incident neutron energy using optical model approaches," EPJ Web of Conf. **146**, 11051 (2017). https://doi.org/10.1051/epjconf/201714611051.

[40] M. Kerveno, M. Dupuis, A. Bacquias *et al.*, "Measurement of $^{238}U(n, n'\gamma)$ cross section data and their impact on reaction models," Phys. Rev. C **104**, 044605 (2021). https://doi.org/10.1103/PhysRevC.104.044605

[41] M.J. Rapp, Y. Danon, F.J. Saglime, R.M. Bahran, D.G. Williams, G. Leinweber, D.P. Barry, R.C. Block *et al.*, "Beryllium and Graphite Neutron Total Cross-Section Measurements from 0.4 to 20 MeV," Nucl. Sci. Eng. **172**, 268–277 (2012). http://dx.doi.org/10.13182/NSE11-55.

[42] S.J. Daugherty, J.B. Albert, L.J. Kaufman *et al.*, "Neutron inelastic scattering measurements on ^{136}Xe at E_n = 0.7 to 100 MeV," Phys. Rev. C **98**, 064606 (2018). http://dx.doi.org/10.1103/PhysRevC.98.064606.

[43] S.M. El-Kadi, C.E. Nelson, F.O. Purser *et al.*, "Elastic and Inelastic Scattering of Neutrons from ^{54,56}Fe and ^{63,65}Cu. (I). Measurements from 8 to 14 MeV and a Spherical Optical Model Analysis," Nucl. Phys. A **390**, 509–540 (1982), http://dx.doi.org/10.1016/0375-9474(82)90281-0.

[44] A.O. Hanson and J.L. McKibben, "A Neutron Detector Having Uniform Sensitivity from 10 keV to 3 MeV," Phys. Rev. **72**, 673–677 (1947). https://doi.org/10.1103/PhysRev.72.673.

[45] R.A. Nobles, R.B. Day, R.L. Henkel *et al.*, "Response of the Long Counter," Rev. Sci. Instrum. **25**, 334–335 (1954). https://doi.org/10.1063/1.1771058.

[46] N.J. Roberts, D.J. Thomas, V. Lacoste *et al.*, "Comparison of Long Counter Measurements of Monoenergetic and Radionuclide Source-based Neutron Fluence," Rad. Meas. **45**, 1151–1153 (2010). https://doi.org/10.1016/j.radmeas.2010.06.046.

[47] H. Tagziria and D.J. Thomas, "Calibration and Monte Carlo Modelling of Neutron Long Counters," Nucl. Instrum. Meth. Phys. Res. Sec. A **452**, 470–483 (2000). https://doi.org/10.1016/S0168-9002(00)00448-4.

[48] H. Klein and F.D. Brooks, "Scintillation Detectors for Fast Neutrons," in *Proc. of Science, International Workshop on Fast Neutron Detectors and Applications, University of Cape Town, South Africa*, (2006). available online at https://pos.sissa.it/025/

[49] H.-J. Kellermann and R. Langkau, "Neutron Detection Efficiency Of The Liquid Scintillator Ne 14 in the MeV Range," Nucl Instrum. Meth. **94**, 137–140 (1971). https://doi.org/10.1016/0029-554X(71)90350-8.

[50] M. Drosg, "Accurate Measurement of the Counting Efficiency of A Ne-213 Neutron Detector between 2 and 26 Me," Nucl. Instrum. Meth. **105**, 573–584 (1972). https://doi.org/10.1016/0029-554X(72)90357-6.

[51] K. Nakayama, E. Farrelly Pessoa and R.A. Douglas, "A Modified Version of the Monte Carlo Computer Code for Calculating Neutron Detection Efficiencies," Nucl. Instrum. Meth. Phys. Res. **190**, 555–563 (1981). https://doi.org/10.1016/0029-554X(81)90956-3.

[52] J. Allison, K. Amako, J. Apostolakis *et al.*, "Geant4 Developments and Applications," IEEE Transactions on Nuclear Science **53**, 270–278 (2006). https://doi.org/10.1109/TNS.2006.869826.

[53] J. Allison, K. Amako, J. Apostolakis *et al.*, "Recent Developments in Geant4," Nucl. Instrum. and Meth. Phys. Res. Sec. A **835**, 186–225 (2016), https://doi.org/10.1016/j.nima.2016.06.125.

[54] J.K. Dickens, "SCINFUL: A Monte Carlo Based Computer Program to Determine a Scintillator Full Energy Response to Neutron Detection for E_n Between 0.1 and 80 MeV: User's Manual and FORTRAN Program Listing," (1988), https://ntrl.ntis.gov/NTRL/dashboard/searchResults/titleDetail/DE88008937.xhtml.

[55] S.A. Pozzi, E. Padovani and M. Marseguerra, "MCNP-PoliMi: a Monte-Carlo Code for Correlation Measurements," Nucl. Instrum. Meth. Phys. Res. Sec. A **513**, 550–558 (2003). https://doi.org/10.1016/j.nima.2003.06.012.

[56] S.A. Pozzi, M. Flaska, A. Enqvist, *et al.*, "Monte Carlo and Analytical Models of Neutron Detection with Organic Scintillation Detectors," Nucl. Instrum. Meth. Phys. Res. Sec. A **582**, 629–637 (2007). https://doi.org/10.1016/j.nima.2007.08.246.

[57] E. Padovani, S.A. Pozzi, S.D. Clarke *et al.*, "MCNPX-PoliMi User's Manual," Oak Ridge National Laboratory Report (2012).

[58] T. N. Massey, S. Al-Quraishi, C.E. Brient *et al.*, "A Measurement of the ^{27}Al(d, n) Spectrum for Use in Neutron Detector Calibration," Nucl. Sci. Eng. **129**, 175–179 (1998). http://dx.doi.org/10.13182/NSE98-A1971.

[59] S. Agostinelli, J. Allison, K. Amako *et al.*, "Geant4—A Simulation Toolkit," Nucl. Instrum. Meth. Phys. Res. Sec. A **506**, 250–303 (2003). https://doi.org/10.1016/S0168-9002(03)01368-8.

[60] W. Mannhart, "Evaluation of the Cf-252 Fission Neutron Spectrum between 0 MeV and 20 MeV," IAEA Report IAEA-TECDOC-410, 158–171 (1987).

[61] W. Mannhart, "Status of the Cf-252 Fission Neutron Spectrum Evaluation with Regard to Recent Experiments," IAEA Report INDC(NDS)-220, 305–336 (1989).

[62] E. Blain, A. Daskalakis, R.C. Block *et al.*, "Measurement of Prompt Fission Neutron Spectrum for Spontaneous Fission of ^{252}Cf using γ Multiplicity Tagging," Phys. Rev. C **95**, 064615 (2017). https://doi.org/10.1103/PhysRevC.95.064615.

[63] N.V. Kornilov, "Verification of the ^{252}Cf Standard in the Energy Range 2–20 MeV," IAEA Report INDC(USA)-108 (2015).

[64] J.W. Meadows, "^{252}Cf Fission Neutron Spectrum from 0.003 to 15.0 MeV," Phys. Rev. **157**, 1076 (1967). https://doi.org/10.1103/PhysRev.157.1076.

[65] K. Gul, A.A. Naqvi and H.A. Al-Juwair, "Relative Neutron Detector Efficiency and Response Function Measurements with a ^{252}Cf Neutron Source," Nucl. Instrum. Meth. Phys. Res. Sec. A **278**, 470–476 (1989). https://doi.org/10.1016/0168-9002(89)90867-X.

[66] H. Marten and D. Seeliger, "Analysis of the Prompt-neutron Spectrum from Spontaneous Fission of ^{252}Cf," J. Phys. G: Nucl. Phys. **10**, 349–362 (1984). https://doi.org/10.1088/0305-4616/10/3/010

[67] M. Herman, A. Trkov, R. Capote *et al.*, "Evaluation of Neutron Reactions on Iron Isotopes for CIELO and ENDF/B-VIII.0," Nucl. Data Sheets **148**, 214–253 (2018). https://doi.org/10.1016/j.nds.2018.02.004.

[68] J. Blok and C.C. Jonker, "A Method for the Computation of Plural and Multiple Scattering Corrections," Physica **18**, 809–822 (1952). https://doi.org/10.1016/S0031-8914(52)80216-2.

[69] C.A. Engelbrecht, "Multiple Scattering Correction for Inelastic Scattering from Cylindrical Targets," Nucl. Instrum. Meth. **80**, 187–191 (1970). https://doi.org/10.1016/0029-554X(70)90760-3.

[70] C.A. Engelbrecht, "Recipes for Multiple Scattering Corrections," Nucl. Instrum. Meth. **93**, 103–107 (1971). https://doi.org/10.1016/0029-554X(71)90145-5.

[71] W.E. Kinney, "Finite-sample Corrections to Neutron Scattering Data," Nucl. Instrum. Meth. **83**, 15–28 (1970). https://doi.org/10.1016/0029-554X(70)90528-8.

[72] D.L. Smith, "Sample-Size Effects in Fast-Neutron Gamma-Ray Production Measurements: Solid Cylinder Samples," Argonne National Laboratory Report ANL/NDM-17 (1975).

[73] M. Salama, O.H. Sallam and K. Naguib, "On the Validity of Cranberg's Analytical Method for Calculation of the Attenuation and Multiple Scattering Corrections," J. Phys. D: Appl. Phys. **16**, 937–942 (1983). http://iopscience.iop.org/0022-3727/16/6/004.

[74] D.E. Velkey *et al.*, "Sample-size Effects in Neutron Scattering Studied with Analytic and Monte Carlo Methods," Nucl. Instrum. Meth. **129**, 231–239 (1975). https://doi.org/10.1016/0029-554X(75)90134-2.

[75] J.R. Lilley, "MULCAT-BRC, A Monte Carlo Neutron and Gamma-Ray Multiple Scattering Correction Program," Internal Service de Physique et Techniques Nucleaire, Centre d'Etudes de Bruyeres-le-Chatel Report P2N/934/80 (1980).

[76] G.F. Auchampaugh, S. Plattard and N.W. Hill, "Neutron Total Cross-section Measurements of ^{9}Be, ^{10,11}B, and ^{12,13}C from 1.0 to 14 MeV Using the ^{9}Be(d,n)^{10}B Reaction as a "White" Neutron Source," Nucl. Sci. Eng. **69**, 30–38 (1979). http://dx.doi.org/10.13182/NSE79-A21282.

[77] M. Drosg, "The ^{1}H(^{7}Li, n)^{7}Be Reaction as a Neutron Source in the MeV Range," Los Alamos National Laboratory Report LA-8842-MS (1981).

[78] M. Drosg, D.M. Drake and J. Mazarik,"Calibration of a Li-glass Detector for Neutron Energies above 50 keV by the ^{1}H(t, n)^{3}He Reaction," Nucl. Instrum. Meth. Phys. Res. Sec. B **94**, 319–324 (1994). https://doi.org/10.1016/0168-583X(94)95371-6.

[79] M. Drosg, R.C. Haight and D.M. Drake, "Double-differential Gamma-ray Production: Cross Sections and Spectra of Al, Si and Fe for 8.51, 10.00, 12.24 and 14.24 MeV Neutrons," Los Alamos National Laboratory Report LA-UR-02-0016 (2002).

[80] M. Drosg, "Novel Monoenergetic Neutron Sources for Energies between 2.5 and 25.7 MeV," Nucl. Instrum. Meth. Phys. Res. Sec. A **254**, 466–468 (1987). https://doi.org/10.1016/0168-9002(87)90701-7

[81] M. Drosg and N. Otuka, "Evaluation of the Absolute Angle-Dependent Differential Neutron Production Cross Sections by the Reactions ^{3}H(p, n)^{3}He, ^{1}H(t, n)^{3}He, ^{2}H(d, n)^{3}He, ^{3}H(d, n)^{4}He, and ^{2}H(t, n)^{4}He and of the Cross Sections of Their Time-Reversed Counterparts up to 30 MeV and Beyond," IAEA INDC(AUS)-0019 (2015).

[82] L. Bernstein, C. Romano, D.A. Brown *et al.*, "Final Report for the Workshop for Applied Nuclear Data Activities,"Lawrence Livermore National Laboratory Report LLNL-PROC-769849 (2019).

[83] A.B. Smith, P. Guenther, R. Larsen *et al.*, "Multi-angle Fast Neutron Time-of-Flight System," Nucl. Phys. **50**, 277–291 (1967). https://doi.org/10.1016/0029-554X(67)90054-7.

[84] M. Lebois, J.N. Wilson, P.Haliprè *et al.*, "Development of a Kinematically Focused Neutron Source with the p(^{7}Li, n)^{7}Be Inverse Reaction," Nucl. Instrum. Meth. Phys. Res. Sec. A **735**, 145–151 (2014). https://doi.org/10.1016/j.nima.2013.07.061.

[85] J. Wilson, M. Lebois and L. Qi, "Neutron-rich Isotopes from ^{238}U(n, f) and ^{232}Th(n, f) Studied with the ν-ball Spectrometer Coupled to the LICORNE Neutron Source," EPJ Web of Conf. **193**, 04010 (2018). https://doi.org/10.1051/epjconf/201819304010

[86] R. Woods, J.L. McKibben and R.L Henkel, "The Los Alamos Three-stage Van de Graaff Facility," Nucl. Instrum. Meth. **122**, 81–97 (1974). https://doi.org/10.1016/0029-554X(74)90473-X.

[87] D.W. Kneff, B.M. Oliver, E. Goldberg *et al.*, "Helium Production Cross Sections for 15-MeV Neutrons on ^{6}Li and ^{7}Li," Nucl. Sci. Eng. **94**, 136 (1986). http://dx.doi.org/10.13182/NSE86-A27448.

[88] M. Drosg, P.W. Lisowski, R.A. Hardekopf *et al.*, "Double Differential Neutron Emission Cross Sections of ^{10}B and ^{11}B at 6, 10 and 14 MeV and of ^{6}Li, ^{7}Li and ^{12}C at 14 MeV," Radiation Effects **92**, 145–149 (1986). https://doi.org/10.1080/00337578608208308.

[89] S. Chiba, M. Mizumoto, K. Hasegawa *et al.*, "The ^{1}H(^{11}B, n)^{11}C Reaction as a Practical Low-background Monoenergetic Neutron Source in the 10 MeV Region," Nucl. Instrum. Meth. Phys. Res. Sec. A **281**, 581–588 (1989). https://doi.org/10.1016/0168-9002(89)91493-9.

[90] D.W. Glasgow, F.O. Perser, H. Hogue, J.C. Clement, K. Selzer, G.Mack, J.R. Boyce, D.H. Epperson, S.G. Buccino, P.W. Lisowski, S.G. Glendinning, E.G. Bilpuch, H.W. Newson, C.R. Gould, "Differential Elastic and Inelastic Scattering of 9- to 15-MeV Neutron from Carbon," Nucl. Sci. Eng. **61**, 521–533 (1976). https://doi.org/10.13182/NSE76-A14488.

[91] A.M. Daskalakis, E.J. Blain, B.J. McDermott *et al.*, "Quasi-differential Elastic and Inelastic Neutron Scattering from Iron in the MeV Energy Range," Annals of Nuclear Energy **110**, 603–612 (2017). https://doi.org/10.1016/j.anucene.2017.07.007.

[92] A.M. Daskalakis, R.M. Bahran, E.J. Blain *et al.*, "Quasi-differential Neutron Scattering from ^{238}U from 0.5 to 20 MeV," Annals of Nuclear Energy **73**, 455–464 (2014). https://doi.org/10.1016/j.anucene.2014.07.023.

[93] D.P. Barry, G. Leinweber, R.C. Block *et al.*, "Quasi-differential Neutron Scattering in Zirconium from 0.5 to 20 MeV," Nucl. Sci. Eng. **174**, 188–201 (2013). http://dx.doi.org/10.13182/NSE12-1.; Numerical values from EXFOR.

[94] J.E. Lynn, "Helios: The New Harwell Electron Linear Accelerator, and its Scientific Programme," Contemporary Physics **21**, 483–500 (2006). https://doi.org/10.1080/00107518008210972.

[95] M.S. Coates, P.P. Thomas, B.P. Clear *et al.*, "A New Linear Accelerator at A.E.R.E Harwell," in *Proc. of the Fourth National Soviet Conference on Neutron Physics, Kiev, U.S.S.R.* **4**, pp. 139–157 (1977).

[96] E. Pirovano, "Neutron Scattering Measurements with a New Scintillator Array, Ph.D Thesis Ghent University " INDC-BLG-0002 (2017). https://www-nds.iaea.org/publications/indc/indc-blg-0002.

[97] K.P. Harrig, B.L. Goldblum, J.A. Brown, D.L. Bleuel, L.A. Bernstein, J. Bevens, M. Harasty, T.A. Laplace, E.F. Matthews, "Neutron Spectroscopy for Pulsed Beams with Frame Overlap using a Double Time-of-Flight Technique," Nucl. Instrum. Meth. Phys. Res. A **877**, 359–366 (2018) https://doi.org/10.1016/j.nima.2017.09.051

[98] K. J. Kelly, E. A. Bennett, M. Devlin, *et al.*, "The Neutron Scattering Cross Section and Angular Distribution Measurement Program at LANL," EPJ Web of Conf. **284**, 01004 (2023) https://doi.org/10.1051/epjconf/202328401004

[99] D. Neudecker, D.L. Smith, F. Tovesson *et al.*, "Applying a Template of Expected Uncertainties to Updating ^{239}Pu(n, f) Cross-section Covariances in the Neutron Data Standards Database," Nucl. Data Sheets, 228–248 (2020). https://doi.org/10.1016/j.nds.2019.12.005.

[100] I. Murata, S. Takaki , K. Shiken *et al.*, "Measurement of the angle-correlated neutron spectrum for the ^{9}Be(n, 2n) reaction with a pencil-beam DT neutron source," Int. Conf. Nucl. Data for Sci. Tech. 07579 (2007). https://dx.doi.org/10.1051/ndata:07579 or http://nd2007.edpsciences.org.

[101] F. J. Saglime, Y. Danon, R. C. Block *et al.*, "A System for Differential Neutron Scattering Experiments in the Energy Range from 0.5 to 20 MeV." Nucl. Instrum. Meth. Phys. Res. A **620**, 401-409 (2010). https://doi.org/10.1016/j.nima.2010.04.051.

[102] A.R. Junghans, R. Beyer, E. Grosse *et al.*, "Fast Neutron Measurements at the nELBE Time-of-flight Facility," EPJ Web of Conf. **93**, 02015 (2015). https://doi.org/10.1051/epjconf/20159302015.

[103] K.J. Kelly, M. Devlin, J.M. O'Donnell, E.A. Bennett, "Correlated $n-\gamma$ angular distributions from the Q=4.4398 MeV ^{12}C(n, n$'\gamma$) reaction for incident neutron energies from 6.5 MeV to 16.5 MeV, " Phys. Rev C **104**, 064614 (2021). https://doi.org/10.1103/PhysRevC.104.064614.

[104] K.J. Kelly, M. Devlin, J.M. O'Donnell, E.A. Bennett, M. Paris, P.A. Copp,"Measurement of the cross section of the Q = 4.4398 MeV ^{12}C(n, n$'\gamma$) reaction from threshold to 16.5 MeV using γ and correlated $n-\gamma$ detection " Phys. Rev C **108**, 014603 (2023). https://doi.org/10.1103/PhysRevC.108.014603

[105] T. Kibédi, T.W. Burrows, M.B. Trzhaskovskaya, *et al.*, "Evaluation of theoretical conversion coefficients using BrIcc," Nucl. Instrum. and Meth. Phys. Res. Sec. A **589** (2008) 202-229.

[106] "Update of X ray and γ ray decay data standards for detector calibration and other applications: recommended decay data, high energy gamma ray standards and angular correlation coefficients," INDC(NDS)-437 Distr. NG+G, (Vienna: International Atomic Energy Agency) (2007).

[107] T. Otuka, E. Dupont, V. Semkova, *et al.* "Towards a More Complete and Accurate Experimental Nuclear Reaction Data Library (EXFOR): International Collaboration Between Nuclear Reaction Data Centres (NRDC), " Nucl. Data Sheets **120**, 272–276, (2014). https://doi.org/10.1016/j.nds.2014.07.065

[108] O. Schwerer *et al.*, "EXFOR Formats Description for Users (EXFOR Basics)," IAEA-NDS-206, (June 2008).

[109] O. Schwerer *et al.*, "EXFOR Formats Description for Users (EXFOR Basics)," IAEA Nuclear Data Section, Vienna, Austria , (June 2007–2023). https://www-nds.iaea.org/nrdc/basics/ and https://www-nds.iaea.org/nrdc/basics/exfor-basics-ap.html#dictionary30

[110] A.M. Lewis *et al.*, "Templates of Expected Measurement Uncertainties for Total Cross Sections,"submitted to Europ. Phys. J. N (2023).

[111] A.J. Koning, S. Hilaire and M.C. Duijvestijn, "TALYS-1.0,", Proceedings of the International Conference on Nuclear Data for Science and Technology, April 22-27, 2007, Nice, France, editors O.Bersillon, F.Gunsing, E.Bauge, R.Jacqmin, and S.Leray, EDP Sciences, 2008, p.211-214.

[112] M. Herman et al., "EMPIRE: Nuclear Reaction Model Code System for Data Evaluation," Nucl. Data Sheets **108**, 2655–2715, (2007). https://doi.org/10.1016/j.nds.2007.11.003

[113] R.L. Walter, "Analyzing power measurements for neutron-nucleus scattering and the spin-orbit potential, " AIP Conference Proceedings **124**, 53–71, (1985). https://doi.org/10.1063/1.34981

[114] A.J. Koning and J.P. Delaroche, "Local and Global Nucleon Optical Models from 1 keV to 200 MeV," Nucl. Phys. A **713**, 231–310 (2003). https://doi.org/10.1016/S0375-9474(02)01321-0.

[115] R. Capote, S. Chiba, E. Soukhovitskii *et al.*, "A Global Dispersive Coupled-channel Optical Model Potential for Actinides," Journal of Nuclear Science and Technology **45**, 333–340 (2008). https://doi.org/10.1080/18811248.2008.9711442.

[116] P. Leconte, D. Bernard, "Validation of the U-238 inelastic scattering neutron cross section through the EXCALIBUR dedicated experiment," EPJ Web of Conf. **146**, 06017 (2017). https://doi.org/10.1051/epjconf/201714606017

[117] R. Capote, A. Trkov, M. Sin, *et al.* "Elastic and Inelastic Scattering of Neutrons on ^{238}U Nucleus," EPJ Web of Conf. **69**, 00008 (2014). https://doi.org/10.1051/epjconf/20146900008

[118] A. Ichihara, S. Kunieda, K. Shibata, "Calculation of Neutron Cross Sections on ^{93}Nb for JENDL-4," j. Nucl. Sci Tech. **45**, 793–801 (2008). https://doi.org/10.1080/18811248.2008.9711480.

[119] V. Avrigeanu, M. Avrigeanu, K "Consistent Accessment of Neutron-Induced Activation of ^{93}Nb," Frontiers in Physics **11**, 1142436 (2023). https://doi.org/10.3389/fphy.2023.1142436.

[120] J. L. Kammerdiener, *Neutron Spectra Emitted by ^{239}Pu, ^{235}U, ^{238}U, Fe, Nb, Ni, Al, and C Irradiated by 14 MeV Neutrons.* PhD thesis, Lawrence Livermore Laboratory Report UCRL-51232 (1972).

[121] P.W. Lisowski, M. Drosg, D.M. Drake, B. Hoop, "Cross Sections for Neutron Production from 6- and 10-MeV Neutrons Incident on 10B and 11B," Nucl. Sci. Eng **195**, 1131–1143 (2021). http://dx.doi.org/10.1080/00295639.2021.1906588

[122] G. Vedrenne, D. Blanc, F. Cambou, "Interaction des neutrons de 14,1 MeV avec le deutérium" J. Phys. France **24**, 801–803 (1963). http://dx.doi.org/10.1051/jphys:019630024011080100

[123] Y.-L. Zhang, X.-C. Ruan, Z.-E. Yao, H.-X. Huang, X. Li, Z.-Y. Zhou, H.-B. Nie, J. Bao , "Measurement of Secondary Neutron Emission Double-differential Cross Section for ^{9}Be Induced by 8.19 MeV Neutrons, " Nucl. Phys. Rev. **28**, 366–370 (2011). http://dx.doi.org/10.11804/NuclPhysRev.28.03.366

[124] R. Han, R. Wada, Z. Chen, *et al.* , "Fast neutron scattering on Gallium target at 14.8 MeV, " Nucl. Phys. A **936**, 17–28 (2015). http://dx.doi.org/10.1016/j.nuclphysa.2015.01.004

[125] Y. Zhang, Y., X. Ruan, X., H. Huang, *et al.* , "Measurement of differential and double-differential neutron emission cross-sections for ^{9}Be at 21.94 MeV neutrons, " Eur. Phys. J. A **53**, 236 (2017). http://dx.doi.org/10.1140/epja/i2017-12434-y

[126] A. Donzella, M. Barbui, F. Bocci, *et al.*, "Evaluation of theoretical conversion coefficients using BrIcc" Nucl. Instrum. and Meth. Phys. Res. Sec. A **613** (2010) 58–64. https://doi.org/10.1016/j.nima.2009.10.135.

[127] J.J. Griffin *et al.*, "Statistical Model of Intermediate Structure," Phys. Rev. Lett. **17**, 478 (1966)." Phys. Rev. Lett. **19**, 57 (1967). https://doi.org/10.1103/PhysRevLett.17.478.

[128] C.M. Perey, F.G. Perey, J.A. Harvey *et al.*, "^{58}Ni + n Transmission, Capture, and Differential Elastic Scattering Data Analysis in the Resonance Region," Radiation Effects **96/14**, 297–300 (1986). https://doi.org/10.1080/00337578608211757.

[129] M.E. Rose, "The Analysis of Angular Correlation and Angular Distribution Data," Phys. Rev. **91**, 610–615 (1953). https://doi.org/10.1103/PhysRev.91.610

[130] R.M. Steffen and H. Frauenfelder, "The Influence of Extranuclear Fields on Angular Correlations," in *Perturbed Angular Correlations Part 1*, edited by E. Karlsson, 13–21 (1964).

[131] W.G. Winn, D.G. Sarantites, "Directional Correlation Attenuation Factors for Ge(LI) γ-Ray Detectors," Nucl. Instrum. Meth. **66**, 61–69 (1968). https://doi.org/10.1016/0029-554X(68)90059-1

[132] C.J. Werner (ed.), "MCNP Users Manual - Code Version 6.2," Los Alamos National Laboratory Report LA-UR-17-29981 (2017).

[133] M. Devlin, J.A. Gomez, K.J. Kelly *et al.*, "The Prompt Fission Neutron Spectrum of ^{235}U(n, f) below 2.5 MeV for Incident Neutrons from 0.7 to 20 MeV," Nucl. Data Sheets **148**, 322–337 (2018). https://doi.org/10.1016/j.nds.2018.02.008.

[134] D. Neudecker, B. Hejnal, F. Torvesson, M.C. White, D.L. Smith, D. Vaughan, R.Capote. "Template for estimating uncertainties of measured neutron-induced fission cross-sections," Europ. Phys. J. N **4**, 21 (2018). https://doi.org/10.1051/epjn/2018026

[135] D. Neudecker, "ARIADNE—A Program Estimating Covariances in Detail for Neutron Experiments," Europ. Phys. J. N **4**, 34 (2018).